

## Identification of Antiferromagnetic Domains Via the Optical Magnetoelectric Effect

Vilmos Kocsis,<sup>1,2</sup> Karlo Penc,<sup>2,3</sup> Toomas Rõõm,<sup>4</sup> Urmas Nagel,<sup>4</sup> Jakub Vít,<sup>2,5,6</sup> Judit Romhányi,<sup>7</sup> Yusuke Tokunaga,<sup>1,8</sup> Yasujiro Taguchi,<sup>1</sup> Yoshinori Tokura,<sup>1,9,10</sup> István Kézsmárki,<sup>2,11</sup> and Sándor Bordács<sup>2,12</sup>

<sup>1</sup>*RIKEN Center for Emergent Matter Science (CEMS), Wako, Saitama 351-0198, Japan*

<sup>2</sup>*Department of Physics, Budapest University of Technology and Economics and MTA-BME Lendület Magneto-optical Spectroscopy Research Group, 1111 Budapest, Hungary*

<sup>3</sup>*Institute for Solid State Physics and Optics, Wigner Research Centre for Physics, Hungarian Academy of Sciences, H-1525 Budapest, P.O.B. 49, Hungary*

<sup>4</sup>*National Institute of Chemical Physics and Biophysics, 12618 Tallinn, Estonia*

<sup>5</sup>*Institute of Physics ASCR, Na Slovance 2, 182 21 Prague 8, Czech Republic*

<sup>6</sup>*Faculty of Nuclear Science and Physical Engineering, Czech Technical University, Břehová 7, 115 19 Prague 1, Czech Republic*

<sup>7</sup>*Okinawa Institute of Science and Technology Graduate University, Onna-son, Okinawa 904-0395, Japan*


<sup>8</sup>*Department of Advanced Materials Science, University of Tokyo, Kashiwa 277-8561, Japan*

<sup>9</sup>*Quantum-Phase Electronics Center, Department of Applied Physics, University of Tokyo, Tokyo 113-8656, Japan*

<sup>10</sup>*Department of Applied Physics, University of Tokyo, Hongo, Tokyo 113-8656, Japan*

<sup>11</sup>*Experimental Physics 5, Center for Electronic Correlations and Magnetism, Institute of Physics, University of Augsburg, 86159 Augsburg, Germany*

<sup>12</sup>*Hungarian Academy of Sciences, Premium Postdoctor Program, 1051 Budapest, Hungary*

 (Received 2 February 2018; revised manuscript received 10 May 2018; published 1 August 2018)

The ultimate goal of multiferroic research is the development of a new-generation nonvolatile memory devices, where magnetic bits are controlled via electric fields with low energy consumption. Here, we demonstrate the optical identification of magnetoelectric (ME) antiferromagnetic (AFM) domains in the  $\text{LiCoPO}_4$  exploiting the strong absorption difference between the domains. This unusual contrast, also present in zero magnetic field, is attributed to the dynamic ME effect of the spin-wave excitations, as confirmed by our microscopic model, which also captures the characteristics of the observed static ME effect. The control and the optical readout of AFM/ME domains, demonstrated here, will likely promote the development of ME and spintronic devices based on AFM insulators.

DOI: [10.1103/PhysRevLett.121.057601](https://doi.org/10.1103/PhysRevLett.121.057601)

During the last few decades, the great potential of multiferroic materials in realizing magnetoelectric (ME) memory devices has led to the revival of the ME effect [1–7] and the discovery of a plethora of multiferroic compounds, including  $\text{BiFeO}_3$ , a well characterized room-temperature multiferroic material [8–10]. In multiferroics-based memory devices, the writing and reading of magnetic bits by electric field may be realized via the ME coupling between the ferromagnetic and ferroelectric orders. Despite the recent progress, the synthesis of multiferroics with magnetization and ME susceptibility sufficiently large for applications is still challenging. As an alternative approach, information could be stored in ME domains even in the absence of ferromagnetism or ferroelectricity. While a similar concept has been proposed for metallic compounds, termed as antiferromagnetic (AFM) spintronics [11], the potential of insulators with coupled antiferromagnetic and antiferroelectric (AFE) orders in ME memories has not been exploited yet.  $\text{LiCoPO}_4$ , being such a multiantiferroic insulator [12], drew such attention, owing to its strong linear ME effect [13,14] and its toroidic order

[15,16]. Here we demonstrate that in the AFM-AFE phase of  $\text{LiCoPO}_4$  the two different ME memory states have distinct optical properties distinguishable by transmission measurements without the need of high-intensity light beams [15,16].

At room temperature,  $\text{LiCoPO}_4$  has the orthorhombic olivine structure (space group:  $Pnma$ ), which is shown in Fig. 1(a). While a local electric polarization is allowed at each Co site due to its low site symmetry, the total polarization of the unit cell vanishes [see Fig. 1(c)]. Below  $T_N = 21.7$  K, this staggered electric polarization is supplemented by a two-sublattice collinear AFM order, where  $S = 3/2$  spins of  $\text{Co}^{2+}$  ions are aligned parallel to the  $y$  axis [17]. Since the AFM state simultaneously breaks the spatial inversion and time reversal symmetries, the material exhibits a linear ME effect ( $P_\mu = \chi_{\mu\nu}^{em} H_\nu$ ,  $\mu, \nu = x, y, z$ ) with finite  $\chi_{xy}^{em}$  and  $\chi_{yx}^{em}$  ME susceptibilities [14]. Although a tiny uniform canting of the spins from the  $y$  axis may further reduce the magnetic symmetry and generate finite  $\chi_{xz}^{em}$  and  $\chi_{zx}^{em}$ , these secondary effects are not relevant to the present study [15,16].

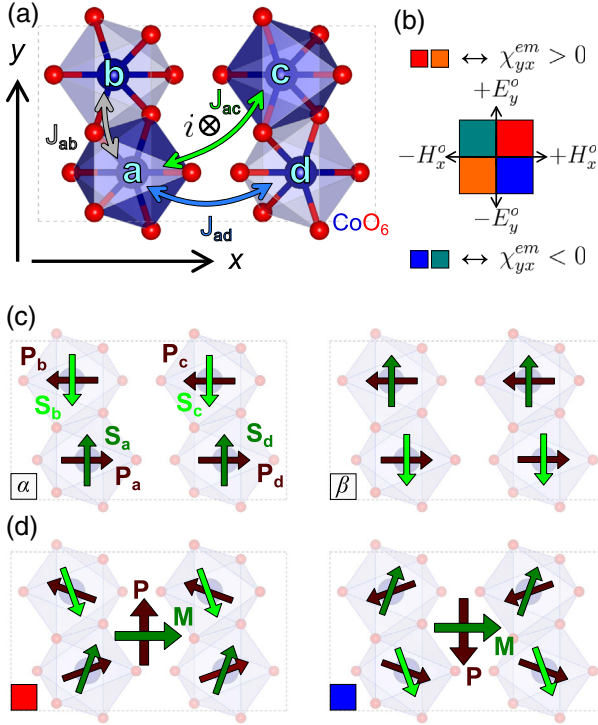


FIG. 1. (a) Unit cell of the LiCoPO<sub>4</sub> viewed from the  $z$  axis. The four Co sites a–d are surrounded by oxygen octahedra, while Li and P sites are omitted for clarity. The inversion center is labeled by  $i$ . The three nonequivalent exchange interactions,  $J_{ab}$ ,  $J_{ac}$ , and  $J_{ad}$ , are indicated with arrows. (b) The four combinations  $(++)$ ,  $(+-)$ ,  $(-+)$ , and  $(--)$  of poling fields  $(H_x, E_y)$  are represented by four colors. (c) The magnetic sublattices (green and olive arrows) in the AFM domains  $\alpha$  and  $\beta$  are interchanged while the AFE polarization pattern (brown arrows) is the same for the two domains. (d) Domains  $\alpha$  and  $\beta$  are selected by the poling fields  $(++)$  (red) and  $(+-)$  (blue) via the ME effect according to Eq. (4), assuming  $c_{2xy} > 0$ .

The two possible AFM domains of LiCoPO<sub>4</sub>, labeled as  $\alpha$  and  $\beta$  in Fig. 1(c), can be transformed into each other by either the spatial inversion or the time reversal operations. They are characterized by static ME coefficients  $\chi_{yx}^{em}$  of opposite signs, as experimentally demonstrated in Figs. 2(a) and 2(b), in agreement with former studies [13,14]. Owing to the ME coupling, simultaneous application of weak crossed fields  $E_y \approx 0.1\text{--}1$  kV/cm and  $\mu_0 H_x \approx 0.1$  T during the cooling process through  $T_N$  establishes a single-domain state. When the sign of either the electric or the magnetic field is reversed the other ME domain is selected [see Figs. 1(b) and 1(d)].

The static ME effect is usually associated with collective modes, the so-called ME resonances [18–20]. These transitions can be excited by both the electric and magnetic fields of light as the magnetic component of the radiation generates not only magnetization but also polarization waves in the material. Depending on the sign of the optical ME effect, the magnetically induced polarization waves can interfere either

constructively or destructively with the polarization waves induced by the electric field of light through the dielectric permittivity, giving rise to an enhancement or reduction of the complex refractive index ( $N = n + i\kappa$ ). For linearly polarized light with  $(\mathbf{E}_y^o, \mathbf{H}_x^o)$  propagating along the  $+z$  direction  $N_{+z}(\omega) = \sqrt{\epsilon_{yy}(\omega)\mu_{xx}(\omega) \pm \chi_{yx}^{em}(\omega)}$ , where  $\epsilon_{yy}$  and  $\mu_{xx}$  are elements of the dielectric permittivity and magnetic permeability tensors and  $\pm$  signs correspond to the two domains with opposite signs of  $\chi_{yx}^{em}(\omega)$  [21]. If the optical ME effect is strong, the ME domain characterized by  $\chi_{yx}^{em}(\omega) < 0$  can become transparent, while for the other domain the absorption coefficient,  $\alpha = 2(\omega/c)\kappa$ , is enhanced. Such unidirectional light transmission, also called directional optical anisotropy, has been reported in several multiferroics [19,21–25]. However, this phenomenon has usually been observed in strong magnetic fields and never as a remanent optical memory effect in zero field. It is important to note that the contrast between the two ME domains has to change sign if light propagation direction is reversed from  $+z$  to  $-z$  according to  $N_{-z}(\omega) = \sqrt{\epsilon_{yy}(\omega)\mu_{xx}(\omega) \mp \chi_{yx}^{em}(\omega)}$ . Thus, the reversal of the light propagation is expected to be equivalent with the interchange of the two domains.

We measured the real and imaginary parts of the refractive index spectra of LiCoPO<sub>4</sub> using time-domain terahertz spectroscopy [26] with linearly polarized light  $(\mathbf{E}_y^o, \mathbf{H}_x^o)$ . The details of the crystal growth are described in the Supplemental Material [27]. Spectra plotted in Figs. 2(c)–2(d) with four different colors were obtained after poling the sample from  $T > T_N$  to  $T = 5$  K using four combinations of the poling fields  $(\pm H_x, \pm E_y)$ , as described for the static ME measurements. To observe the remanent effects, the fields were switched off during the spectroscopic measurements. Below  $T_N$  two strong resonances of magnetic origin appear at 1.13 THz and 1.36 THz. The strength of the resonance at 1.36 THz strongly depends on the poling conditions, namely it is weak for the same signs and strong for the opposite signs of poling fields. Moreover, the two spectra obtained for the same sign of poling fields are identical within the precision of the experiment as well as the two spectra measured with poling fields of opposite signs. This indicates the strong ME character of the mode at 1.36 THz, and it also demonstrates the realization of either of the two ME domain states after the poling process. In contrast, the mode at 1.13 THz shows only a weak optical ME effect, with an opposite sign compared to the mode at 1.36 THz.

Next, we verified that the optical contrast between the two ME domains changes upon the reversal of light propagation direction as expected on symmetry grounds. Indeed, as discerned in Figs. 2(e)–2(f), spectra measured for light propagation along the  $+z$  direction with the same sign of poling fields coincide with spectra measured for light propagation along the  $-z$  direction with opposite signs

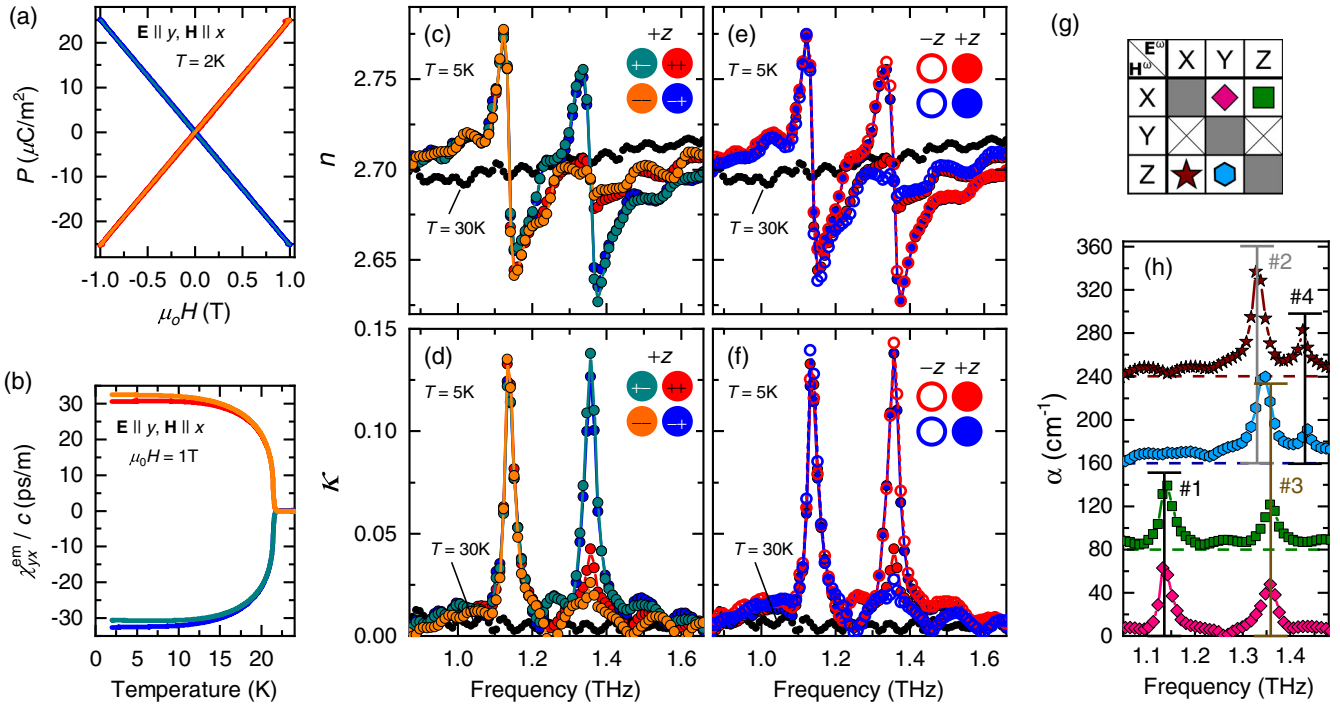


FIG. 2. (a) Magnetic field dependence of the static ME effect at  $T = 2\text{ K}$  measured after poling the sample in the four combinations  $(++)$ ,  $(+-)$ ,  $(-+)$  and  $(--)$  of poling fields  $(H_x, E_y)$ . The poling fields were switched off during the measurement; hence, the linear slope of the polarization ( $P$ ) versus magnetic field curve shows the linear ME effect. (b) Temperature dependence of the linear ME effect,  $\chi_{yx}^{em}$ , measured in warming up after poling in the four configurations of  $(H_x, E_y)$ . Spectra of the (c) real and (d) imaginary part of the refractive index at  $T = 5\text{ K}$  measured after poling. Spectra of the (e) real and (f) imaginary part of the refractive index measured at  $T = 5\text{ K}$  after poling in two selected configurations,  $(++)$  and  $(+-)$  and for light propagation along the  $+z$  direction (full symbols) and the  $-z$  direction (open symbols). The spectra in (c)–(f) were measured using linearly polarized light with  $(\mathbf{E}^\omega, \mathbf{H}^\omega)$ . Spectra measured in the paramagnetic state are plotted in black. The color of each curve corresponds to the applied poling process following the convention introduced in Fig. 1. (h) Selection rules of the spin-wave excitations in  $\text{LiCoPO}_4$ . Absorption coefficient spectra measured in six different polarization configurations of electric ( $\mathbf{E}^\omega$ ) and magnetic ( $\mathbf{H}^\omega$ ) fields according to table (g). In four spectra, shifted vertically for clarity, four distinct resonances are identified and labeled as modes #1 to #4. No absorption peak was observed for  $\mathbf{H}^\omega \parallel y$  (not displayed). The black vertical bars, indicating the positions of these resonances, cross only those spectra where the corresponding resonances are active. The red spectrum, corresponding to the case where the optical ME effect was observed is an average of the four different poling combinations.

of the poling fields. Because of the optical ME effect, for a given direction of light propagation one of the ME domains is nearly transparent at around 1.36 THz, while the other domain strongly absorbs photons in this frequency range, as reflected by the large difference in  $\kappa$ . Note that, this difference corresponds to a factor of  $\approx 300$  in the light intensity transmitted by the two domains for sample of 1 mm thickness.

In order to systematically determine the selection rules for the two spin-wave modes shown in Fig. 2 and to check the existence of other spin-wave excitations, optical absorption spectra were measured for light propagation along the  $x$ ,  $y$  and  $z$  axes, with two orthogonal linear polarizations in each case. In the absence of poling, averaging over the different ME domains eliminates the directional optical anisotropy term from the refractive index; hence,  $N(\omega) = \sqrt{\epsilon_{\mu\mu}(\omega)\mu_{\nu\nu}(\omega)}$ . As shown in Fig. 2(h), besides the two modes coupled to  $\mathbf{H}_x^\omega$  (#1 and #3) we observed two additional spin-wave resonances coupled to  $\mathbf{H}_z^\omega$  at

1.33 THz (#2) and 1.43 THz (#4), while no resonance was detected for  $\mathbf{H}_y^\omega$ . The directional optical anisotropy, found to be strong for mode #3 and weak for mode #1 [Figs. 2(c)–2(f)], requires that these resonances respond to both  $\mathbf{E}_y^\omega$  and  $\mathbf{H}_x^\omega$ . Indeed, the contribution of mode #3 to the  $(\mathbf{E}_y^\omega, \mathbf{H}_z^\omega)$  spectrum [blue in Fig. 2(h)] can only be explained by the electric dipole excitation of this resonance via  $\mathbf{E}_y^\omega$ .

In our theoretical model, we consider the following Hamiltonian for the spins  $S_a, S_b, S_c, S_d$  in the unit cell, imposed by the space group symmetry of  $\text{LiCoPO}_4$  (see the Supplemental Material and Refs. [30–32]):

$$\begin{aligned}
 \mathcal{H} = & 4J_{ij} \sum_{\langle ij \rangle} \mathbf{S}_i \cdot \mathbf{S}_j - \Lambda_{y^2} \sum_i (S_i^y)^2 - \Lambda_{x^2-z^2} \sum_i Q_i^{x^2-z^2} \\
 & - \Lambda_{2xz} (Q_a^{2xz} - Q_b^{2xz} + Q_c^{2xz} - Q_d^{2xz}) \\
 & - g_{xx} \mu_B H_x \sum_i S_i^x - E_y P_y,
 \end{aligned} \quad (1)$$



where  $i \in \{a, b, c, d\}$ .  $J_{ij}$  is the nearest neighbour exchange coupling with  $J_{ab} = J_{cd}$ ,  $J_{ac} = J_{bd}$ , and  $J_{ad} = J_{cb}$ , see Fig. 1(a). The  $\Lambda_{y^2}$ ,  $\Lambda_{x^2-z^2}$ , and  $\Lambda_{2xz}$  are the single-ion anisotropy parameters and the spin-quadrupole terms are defined as  $Q_i^{x^2-z^2} = S_i^x S_i^x - S_i^z S_i^z$  and  $Q_i^{2\mu\nu} = S_i^\mu S_i^\nu + S_i^\nu S_i^\mu$ . The last line of Eq. (1) describes the interaction with static magnetic and electric fields, where the electric polarization is calculated following Refs. [33,34],

$$P_y = c_{2xy}(Q_a^{2xy} - Q_b^{2xy} - Q_c^{2xy} + Q_d^{2xy}) + c_{2yz}(Q_a^{2yz} + Q_b^{2yz} - Q_c^{2yz} - Q_d^{2yz}), \quad (2)$$

with the coefficients  $c_{2xy}$  and  $c_{2yz}$  characterizing the strength of the magnetoelectric coupling.

A finite  $H_x$  cants the ordered spins, and the nonzero  $S_y$  and  $S_x$  components produce a finite electric polarization  $P_y$  whose sign depends on the domain, as shown in Fig. 1(d). The ground state energies of the two AFM domains are calculated using a variational approach [27],

$$E_{GS}(\alpha/\beta) \approx -18(J_{ab} + J_{ac} + J_{ad}) - 9\Lambda_{y^2} - \frac{3(2c_{2xy}E_y \pm g_{xx}\mu_B H_x)^2}{2(6J_{ab} + 6J_{ac} + \Lambda_{y^2})}, \quad (3)$$

where  $\pm$  signs correspond to domain  $\alpha$  and  $\beta$ , respectively. As shown in Fig. 3(a), in crossed electric and magnetic fields the degeneracy of the two AFM domains is lifted and  $\alpha$  is selected when  $E_y H_x > 0$ , while  $\beta$  for  $E_y H_x < 0$ . Correspondingly, the ME susceptibility for domain  $\alpha$  and  $\beta$  has opposite sign,

$$\chi_{yx}^{em}(\alpha/\beta) = \pm \frac{6c_{2xy}g_{xx}\mu_B}{6J_{ab} + 6J_{ac} + \Lambda_{y^2}}, \quad (4)$$

in accordance with the experiment [Figs. 2(a) and 2(b)].

The oscillating magnetization ( $\mathbf{M}^\omega$ ) and polarization ( $\mathbf{P}^\omega$ ) of the spin excitations with  $\Delta S = 1$  over the ground state were characterized by multiboson spin-wave theory [27]. In agreement with our THz spectroscopy experiments, two ME excitations were found with  $\mathbf{M}_x^\omega$  and  $\mathbf{P}_y^\omega$ , from which  $|\pi\pi\rangle$  is assigned to mode #1 and  $|\pi 0\rangle$  to mode #3. Two further modes,  $|0\pi\rangle$  and  $|00\rangle$ , are excited with  $\mathbf{H}_z^\omega$ . They are associated with no finite  $\mathbf{P}^\omega$  and are assigned to modes #2 and #4. Motion of the sublattice magnetizations and local polarizations according to Eq. (2) are illustrated in Figs. 3(b) and 3(c). The finite  $\mathbf{P}^\omega$  of the ME excitations is attributed to the uncompensated polarization of the unit cell [Fig. 3(b)], whereas the local dynamic polarization is canceled for the  $|0\pi\rangle$  and  $|00\rangle$  modes within the  $yz$  layers [Fig. 3(c)]. While the spin components precess in the same direction in  $\alpha$  and  $\beta$  domains, there is a  $\pi$  phase shift between oscillations of  $\mathbf{P}_y^\omega$  in the two domains, as Eq. (2) is linear in the sublattice magnetization along the  $y$  axis. This

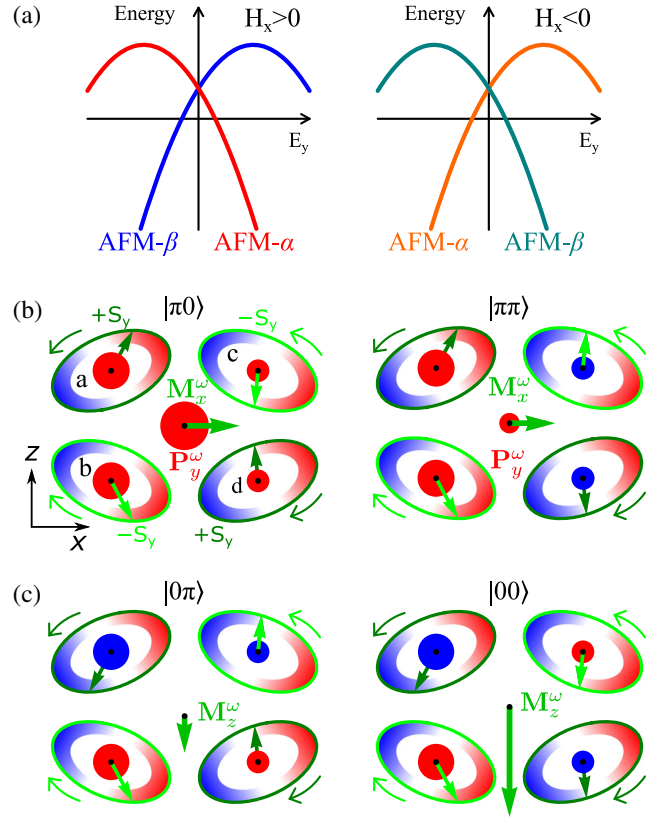


FIG. 3. (a) Energies of the AFM domains are quadratic in the electric and magnetic fields according to Eq. (3). When  $H_x > 0$ , the  $\alpha$  domain has lower energy than the  $\beta$  for positive  $E_y$ , while negative  $E_y$  stabilizes the  $\beta$  domain. For  $H_x < 0$ , the roles of the two AFM domains are interchanged. Schematic drawing of the (b) magnetoelectric ( $\mathbf{P}_y^\omega$ ,  $\mathbf{M}_x^\omega$ ) and (c) magnetic only ( $\mathbf{M}_z^\omega$ ) spin excitations in the  $\alpha$  domain, viewed from the  $y$  axis. Local magnetization of the a and c sites precess counterclockwise along alternately rotated ellipses in the  $xz$  plane, while on the b and d sites spins precess clockwise. The red and blue shading around the ellipses represents the  $y$  component of the local polarization, while the green edge shows the path swept by the  $xz$  component the local magnetization. In the center of each ellipse, the actual direction of the precessing spin is shown by green arrows, while the red and blue marks represent the actual value of the spin-induced polarization. When the precessing spin points to the red (blue) region, the polarization is pointing in the  $+y$  ( $-y$ ) axis, while magnitude of the polarization is illustrated by the size of the mark. The resultant oscillating net magnetic ( $\mathbf{M}_x^\omega$  and  $\mathbf{M}_z^\omega$ ) and net electric ( $\mathbf{P}_y^\omega$ ) dipole moments are shown in the middle of each unit cell. For  $\beta$  domains red and blue shading of the ellipses are reversed; hence,  $\mathbf{P}_y^\omega$  is in antiphase compared to the  $\alpha$  domain.

sign change of the dynamic polarization is the microscopic origin of the optical directional anisotropy in  $\text{LiCoPO}_4$ .

By comparing the strength of the optical ME effect for the different transitions, as experimentally observed and as predicted by our theory, we reveal the dominant mechanism responsible for the spin-induced polarization along the  $y$  axis. Namely, the leading term in  $P_y$  is the one with coefficient  $c_{2yz}$ , giving rise to the strong optical ME

mode #3. The other term in  $P_y$  with coefficient  $c_{2xy}$  is negligible, as almost no optical ME effect was observed for mode #1.

{See Eq. (2) in the main text and Eqs. (6b), (59) and (60) in the Supplemental Material [27]}. The other symmetry allowed component of the ME tensor,  $\chi_{xy}^{em}$ , found finite in the static limit [14], implies the existence of other transitions with nonvanishing  $\mathbf{M}_y^\omega$  and  $\mathbf{P}_x^\omega$  owing to the ME sum rule [18]. Such additional excitations, captured by our theory in the Supplemental Material, are out of the spectral window of the current study.

In summary, we demonstrated that the ME effect can be exploited not only for the control but also for the optical identification of AFM domains as the dynamic ME effect can give rise to a sizeable absorption difference between AFM domains even in zero magnetic field. Our microscopic theory, identifying the main microscopic mechanism behind the ME effect in orthorhombic LiCoPO<sub>4</sub>, implies that the same effect arises in other AFM materials, e.g., compounds belonging to the tetragonal  $4/m'mm$  point group as examples of a higher symmetry case. We expect our study will motivate search for multiantiferroic materials. Moreover, the same principle can also be used for the imaging of AFM domains with micrometer resolution in these materials via conventional optical absorption measurements.

This work was supported by the Hungarian Research Funds OTKA K 108918, by the National Research, Development and Innovation Office NKFIH Grants No. ANN 122879 and No. K 124176, by the BME-Nanotechnology and Materials Science FIKP grant of EMMI (BME FIKP-NAT), by the Deutsche Forschungsgemeinschaft (DFG) via the Transregional Research Collaboration TRR 80: From Electronic Correlations to Functionality (Augsburg—Munich—Stuttgart), by the Estonian Ministry of Education and Research under Grant No. IUT23-03, and the European Regional Development Fund project TK134.

---

[1] M. Fiebig, T. Lottermoser, D. Meier, and M. Trassin, *Nat. Rev. Mater.* **1**, 16046 (2016).  
 [2] S. Dong, J.-M. Liu, S.-W. Cheong, and Z. Ren, *Adv. Phys.* **64**, 519 (2015).  
 [3] T. Kimura, T. Goto, H. Shintani, K. Ishizaka, T. Arima, and Y. Tokura, *Nature (London)* **426**, 55 (2003).  
 [4] M. Fiebig, *J. Phys. D* **38**, R123 (2005).  
 [5] N. A. Spaldin and M. Fiebig, *Science* **309**, 391 (2005).  
 [6] W. Eerenstein, N. D. Mathur, and J. F. Scott, *Nature (London)* **442**, 759 (2006).  
 [7] S.-W. Cheong and M. Mostovoy, *Nat. Mater.* **6**, 13 (2007).  
 [8] J. T. Henron *et al.*, *Nature (London)* **516**, 370 (2014).  
 [9] D. Sando *et al.*, *Nat. Mater.* **12**, 641 (2013).

[10] I. Kézsmárki, U. Nagel, S. Bordács, R. S. Fishman, J. H. Lee, H. T. Yi, S. W. Cheong, and T. Rõm, *Phys. Rev. Lett.* **115**, 127203 (2015).  
 [11] T. Jungwirth, X. Marti, P. Wadley, and J. Wunderlich, *Nat. Nanotechnol.* **11**, 231 (2016).  
 [12] LiCoPO<sub>4</sub> may rather be called antipyroelectric, since its staggered polarization is linked to its crystal structure and may exist up to its melting point. However, this terminology is not common in the literature, thus, the term antiferroelectric is used throughout the text.  
 [13] M. Mercier, J. Gareyte, and E. F. Bertaut, *C. R. Acad. Sci. Ser. B* **264**, 979 (1967).  
 [14] J.-P. Rivera, *Ferroelectrics* **161**, 147 (1994).  
 [15] B. B. Van Aken, J.-P. Rivera, H. Schmid, and M. Fiebig, *Nature (London)* **449**, 702 (2007).  
 [16] A. S. Zimmermann, D. Meier, and M. Fiebig, *Nat. Commun.* **5**, 4796 (2014).  
 [17] R. P. Santoro, D. J. Segal, and R. E. Newnham, *J. Phys. Chem. Solids* **27**, 1192 (1966).  
 [18] D. Szaller, S. Bordács, V. Kocsis, T. Rõm, U. Nagel, and I. Kézsmárki, *Phys. Rev. B* **89**, 184419 (2014).  
 [19] I. Kézsmárki, N. Kida, H. Murakawa, S. Bordács, Y. Onose, and Y. Tokura, *Phys. Rev. Lett.* **106**, 057403 (2011).  
 [20] S. Miyahara and N. Furukawa, *J. Phys. Soc. Jpn.* **81**, 023712 (2012).  
 [21] I. Kézsmárki *et al.*, *Nat. Commun.* **5**, 3203 (2014).  
 [22] S. Bordács *et al.*, *Nat. Phys.* **8**, 734 (2012).  
 [23] M. Saito, K. Ishikawa, K. Taniguchi, and T. Arima, *Phys. Rev. Lett.* **101**, 117402 (2008).  
 [24] Y. Takahashi, R. Shimano, Y. Kaneko, H. Murakawa, and Y. Tokura, *Nat. Phys.* **8**, 121 (2012).  
 [25] S. Bordács, V. Kocsis, Y. Tokunaga, U. Nagel, T. Rõm, Y. Takahashi, Y. Taguchi, and Y. Tokura, *Phys. Rev. B* **92**, 214441 (2015).  
 [26] N. Vieweg, F. Rettich, A. Deninger, H. Roehle, R. Dietz, T. Göbel, and M. Schell, *J. Infrared Milli. Terahz. Waves* **35**, 823 (2014).  
 [27] See Supplemental Material at <http://link.aps.org/supplemental/10.1103/PhysRevLett.121.057601> for further information concerning the crystal growth, the space group symmetry and the Hamiltonian, the variational treatment, the multiboson spin-wave theory, and the fitting procedure. This includes Refs. [28,29].  
 [28] R. Saint-Martin and S. Franger, *J. Cryst. Growth* **310**, 861 (2008).  
 [29] M. Akaki, D. Yoshizawa, A. Okutani, T. Kida, J. Romhányi, K. Penc, and M. Hagiwara, *Phys. Rev. B* **96**, 214406 (2017).  
 [30] W. Tian, J. Li, J. W. Lynn, J. L. Zarestky, and D. Vaknin, *Phys. Rev. B* **78**, 184429 (2008).  
 [31] S. Miyahara and N. Furukawa, *J. Phys. Soc. Jpn.* **80**, 073708 (2011).  
 [32] K. Penc *et al.*, *Phys. Rev. Lett.* **108**, 257203 (2012).  
 [33] T. Arima, *J. Phys. Soc. Jpn.* **76**, 073702 (2007).  
 [34] J. Romhányi, M. Lajkó, and K. Penc, *Phys. Rev. B* **84**, 224419 (2011).